Submitted to *Progress in Surface Science*

Quantitative Prediction of Surface Segregation in Bimetallic Pt-M Alloy Nanoparticles (M=Ni, Re, Mo)

Guofeng Wang [1], M. A. Van Hove [1,2,3,*], P. N. Ross [1], and M. I. Baskes [4]

[1] Materials Sciences Division, Lawrence Berkeley National Laboratory, University of California, Berkeley, CA 94720

[2] Advanced Light Source, Lawrence Berkeley National Laboratory, University of California, Berkeley, CA 94720

[3] Department of Physics, University of California, Davis, CA 95616

[4] MST-8 Structure and Property Relations Group, Los Alamos National Laboratory, Los Alamos, NM 87545

[*] Corresponding author. Tel: 510-486-6160; Fax: 510-486-5530.
E-mail address: MAVanHove@lbl.gov (M.A. Van Hove)

Abstract – This review addresses the issue of surface segregation in bimetallic alloy nanoparticles, which are relevant to heterogeneous catalysis, in particular for electro-catalysts of fuel cells. We describe and discuss a theoretical approach to predicting surface segregation in such nanoparticles by using the Modified Embedded Atom Method and Monte Carlo simulations. In this manner it is possible to systematically explore the behavior of such nanoparticles as a function of component metals, composition, and particle size, among other variables. We chose to compare $Pt_{75}Ni_{25}$, $Pt_{75}Re_{25}$, and $Pt_{80}Mo_{20}$ alloys as example systems for this discussion, due to the importance of Pt in catalytic processes and its high-cost. It is assumed that the equilibrium nanoparticles of these alloys have a cubo-octahedral shape, the face-centered cubic lattice, and sizes ranging from 2.5 nm to 5.0 nm. By investigating the segregation of Pt atoms to the surfaces of the nanoparticles, we draw the following conclusions from our simulations at T= 600 K. (1) $Pt_{75}Ni_{25}$ nanoparticles form a surface-sandwich structure in which the Pt atoms are strongly enriched in the outermost and third layers while the Ni atoms are enriched in the second layer. In particular, a nearly pure Pt outermost surface layer can be achieved in those nanoparticles. (2) Equilibrium $Pt_{75}Re_{25}$ nanoparticles adopt a core-shell structure: a nearly pure Pt shell surrounding a more uniform Pt-Re core. (3) In $Pt_{80}Mo_{20}$ nanoparticles, the facets are fully occupied by Pt atoms, the Mo atoms only appear at the edges and vertices, and the Pt and Mo atoms arrange themselves in an alternating sequence along the edges and vertices. Our simulations quantitatively agree with previous experimental and theoretical results for the extended surfaces of Pt-Ni, Pt-Re, and Pt-Mo alloys. We further discuss the reasons for the different types of surface segregation found in the different alloys, and some of their implications.

Keywords: surface segregation; Modified Embedded Atom Method; Monte Carlo method; nanoparticle; Platinum; Nickel; Rhenium; Molybdenum.

1. Introduction

Surface segregation refers to the phenomenon by which the chemical composition at the surface of multi-component materials differs from the composition in the bulk. Surface segregation has drawn much attention because it influences such materials properties as adsorption, wetting, oxidation and corrosion, electrical contact, friction and wear, catalysis, etc. [1-3]. Theoretical approaches yielding predictions of surface segregation in materials (especially alloys) have long been pursued [4-10]. Phenomenological theories (for example, [5, 6]) incorporate such factors as the heat of solution of alloys, the difference in the pure metal surface energies, and the atom size mismatch in their description of the surface segregation in extended surfaces. In contrast, microscopic theories of surface segregation involve evaluating the system energy (for example, tight-binding theory in [8], embedded atom method (EAM) in [9], and density functional theory in [10]) and a statistical mechanics method to determine the equilibrium properties of alloy surfaces.

Although phenomenological theories are only able to yield qualitative predictions of the surface segregation behavior in alloys, they are very helpful in understanding the physical origins of surface segregation processes. In randomly ordered bimetallic alloys, surface segregation must lower the Gibbs energy of the alloy systems. Therefore, (1) the majority component will segregate to the surface if its heat of solution is negative; (2) the component with the lower surface energy will be driven to the surface; and (3) that component which most decreases strain energies in the surface will segregate to the surface when atomic size-mismatch is appreciable. Microscopic theories are able to provide quantitative predictions of the surface segregation if the important thermodynamic properties of alloys are implicitly and accurately incorporated in the energy evaluation models. In comparison to phenomenological theories, microscopic theories are especially advantageous in predicting surface segregation in alloy nanoparticles. This success is because microscopic theories can explicitly take the geometry, size, and relaxation of nanoparticles into account. Moreover, microscopic theories can include the interactions between the neighboring facets, edges, and vertices of nanoparticles. We have recently developed a microscopic approach to predicting

surface segregation in extended alloy surfaces, by combining the modified embedded atom method (MEAM) [11,12] for energy evaluation and the Monte Carlo (MC) method [13] as the model of statistical mechanics. We have also successfully applied this approach to investigating surface segregation phenomena in bimetallic alloy nanoparticles containing platinum (Pt), as described below.

Metal nanoparticles are extensively studied due to their optical [14], electronic [15], magnetic [16], catalytic [17], and biomedical [18] applications. The unique chemical and physical properties of metal nanoparticles are determined by their size, shape, crystal structure, composition, and surface structure. The surface composition of metal nanoparticles is particularly important for their catalytic applications. For bimetallic nanoparticles, surface segregation means that one alloy component will be enriched in the surface region. Therefore, it would be economically attractive to design bimetallic catalyst nanoparticles in which the precious and catalytic metal atoms segregate to the surface. Pt has been used widely as a catalyst. In particular, Pt is very unique in facilitating the oxygen reduction reaction that is an essential electrochemical process in low temperature polymer electrolyte fuel cells (PEFCs) [19, 20]. However, Pt is a precious metal and has limited availability. To lower the cost of fuel cells, it is desirable to design new electrode catalysts containing a low Pt content overall, but high Pt concentration in the surface. To this end, we chose to theoretically investigate the segregation tendency of Pt atoms to the surfaces of Pt-Ni [21], Pt-Re [22], and Pt-Mo [23] nanoparticles.

Pt-Ni, Pt-Re, and Pt-Mo alloys are catalytic materials of interest for their applications as electro-catalysts in PEFCs. It has been reported that the Pt-Ni alloy catalysts even have enhanced activity compared to pure platinum catalysts as cathodes in PEFCs, depending on how the surfaces are prepared [24]. Early work on electro-oxidation of H_2, CO and H_2/CO mixtures with Pt-Re bulk alloy electrodes also indicates that Pt-Re catalysts could be an economical choice as electro-catalysts in PEFCs [25]. Further experimental [26] and theoretical [20, 27] studies indicate that the oscillatory surface segregation in Pt-Ni alloys may be responsible for the enhancement of their catalytic performance. Therefore, it is helpful to accurately characterize the surface segregation in those alloy nanoparticles in order to design low-cost yet good-performance catalysts for fuel cells. The Pt-Mo alloy

is a promising candidate for CO-tolerant anode catalysts in PEFCs. It was reported that there is an optimal composition for Pt-Mo alloy catalysts to yield best catalytic performance for the electro-oxidation of H_2 and H_2/CO mixtures [28]. This is consistent with the idea of a "bi-functional mechanism": CO adsorbed on Pt could be only oxidized by a neighboring oxygen-containing surface species adsorbed on Mo [29]. Hence, it is of practical use to simulate the arrangement of Pt and Mo atoms in the surface of Pt-Mo catalyst nanoparticles.

Bimetallic nanoparticles can be characterized by such experimental techniques as transmission electron microscopy (TEM), ultraviolet/visible (UV/VIS) spectroscopy, and X-Ray methods [30]. Among various experimental choices, extended x-ray absorption fine structure (EXAFS) is one of the most powerful methods for quantifying the surface segregation of bimetallic nanoparticles. EXAFS measures backscattering photoelectrons with energies above the absorption edge of a component element in nanoparticles and yields information about the atomic number, neighbor distances and coordination number of the element whose absorption edge is being examined [31]. For example, it was deduced using EXAFS data that Pt-Pd [32] and Pt-Ru [33] nanoparticles exhibit core-shell structures (in which one component segregates to the surface shell and hence is depleted in the core). Despite much success, EXAFS demands synchrotron facilities that are not widely accessible.

As an alternative to experimental measurements, atomistic simulations can be used to analyze surface segregation in bimetallic nanoparticles [34,35]. However, most theoretical models for metallic systems only work properly for those metals whose equilibrium structure assumes the face-centered cubic (fcc) lattice. As a result, most previous studies (for example, [36-39]) were limited to fcc-fcc bimetallic systems. By including angular terms into the original EAM [40,41], Baskes made it possible to develop MEAM potentials [11,12] that are also applicable to metals that prefer body-centered cubic (bcc) and hexagonal closed-packed (hcp) structures. Furthermore, MEAM potentials can yield more accurate predictions for bcc metals by including the interactions between second nearest neighbors, whose distances are only about 15 % larger than the separations between the first nearest neighbors in bcc crystals [42,43]. Therefore, one aim of our investigations for Pt-Ni (fcc-fcc), Pt-Re (fcc-hcp), and Pt-Mo (fcc-bcc)

nanoparticles is to establish that the MEAM approach is capable of accurately simulating surface phenomena for a broad spectrum of Pt bimetallic alloy nanoparticles, even when one component might prefer a different lattice. Using MEAM potentials, we have indeed achieved reasonably good simulation results for Pt-rich Pt-Ni [21], Pt-Re [22], and Pt-Mo [23] nanoparticles with the fcc lattices and Re-rich Pt-Re [22] nanoparticles with the hcp lattice.

2. Theoretical methods

2.1. Modified Embedded Atom Method

Within MEAM, the total energy of a system is calculated as

$$E = \sum_i \left[F(\overline{\rho}_i) + \frac{1}{2} \sum_{j(\neq i)} \Phi(R_{ij}) \right] \quad (1)$$

On the right-hand side of Eq. 1, the first term is the embedding energy for atom i which is embedded in the electron density $\overline{\rho}_i$, and the second term is the core-core pair repulsion between atoms i and j separated by a distance R_{ij}. The embedding energy term includes many-body effects, which are very significant for transition metals. $\overline{\rho}_i$ is the background electron density at the center of atom i obtained by the superposition of electronic densities from its surrounding atoms. In EAM, unlike MEAM, the electron density of atoms is only dependent on atomic separations. As an improvement, the electron density of atoms in MEAM consists of both radially and angularly dependent contributions from neighboring atoms. The detailed description of the MEAM formalism has been presented in the literature [11, 12].

The MEAM potentials for the pure metals (Pt, Ni, Re, and Mo) are developed by fitting parameters to reproduce empirical data for cohesive energies, lattice constants, elastic constants, and vacancy formation energies of fcc Pt, fcc Ni, hcp Re, and bcc Mo [21-23]. Moreover, as shown in Table 1, the MEAM potentials for pure metals lead to surface energies of relaxed extended low-index pure surfaces that are in good agreement with first-principles calculations [44] and experimental measurements [45, 46]. The relative surface energies of pure metallic components are major factors that influence the surface segregation phenomena in alloy systems. To determine the cross potentials

between Pt and M (M=Ni, Re, and Mo), we chose Pt_3M (which adopts the $L1_2$ structure) as the reference structure and fitted MEAM potentials to first-principles calculation results of Pt_3M ($L1_2$). Hence, the Pt-M pair potential can be evaluated using the formalisms given in Ref. [47]. The parameters of MEAM potentials for Pt-Ni, Pt-Re, and Pt-Mo bimetallic alloys have already been published [21-23].

2.2. Monte Carlo method

We used the Monte Carlo (MC) approach [13] to drive nanoparticles toward their equilibrium state at finite temperature. In our MC simulations of bimetallic Pt-M nanoparticles, we kept the total number of atoms of each element and the simulation temperature constant. Starting from an atomic configuration within a perfect unrelaxed cubo-octahedron, we perform a series of configuration transformations to achieve thermodynamically equilibrated states. In the equilibrium stage of our MC simulations, the configurations are generated in proportion to the probability of a configuration occurring in an equilibrium canonical ensemble. The physical quantities of interest, such as Pt concentrations in the surface or core of nanoparticles, are obtained by averaging over many equilibrium configurations.

In each MC step, one of the following two configuration changes is attempted with an equal probability: (1) a randomly selected atom is displaced from its original position in a random direction, and (2) two randomly selected atoms with different element types are exchanged. Operation (1) accounts for the positional relaxation processes (adjustment of bond lengths and angles), while operation (2) accounts for the compositional relaxation processes (segregation) in the nanoparticles. In operation (1), the magnitude of the atomic displacement lies in the range $(0, r_{max}]$. At a given temperature, the maximum displacement r_{max} is tuned so that the acceptance probability of new configurations is about 0.5 during the equilibrated part of the simulations.

After each configuration change, we evaluate the energy change ΔE between the new and old configurations. If the configuration change decreases the energy, the new configuration is always retained; while if the configuration change increases the energy, the new configuration is retained with a probability P given by

$$P = \exp(-\frac{\Delta E}{k_B T}) \quad (2)$$

where k_B is the Boltzmann constant and T is the simulation temperature.

In the beginning of MC simulations, the potential energy of Pt-M nanoparticles decreases rapidly due to positional and compositional relaxations. Moreover, the acceptance rate of element exchange operations is rather high as a result of surface segregation processes. In contrast, when the simulations approach equilibrium, there is no significant change in potential energy and the acceptance rate of element exchange operations remains stable around a certain (usually small) value. In this work, we chose the total length of the MC simulations to be twice the number of MC steps required for the largest Pt-M nanoparticle to achieve equilibrium under our criterion.

3. Prediction of surface segregation in nanoparticles

3.1. Overview

The surface segregation in bimetallic nanoparticles is influenced by their component elements, composition, crystal lattice, shape, and size. In this review, we discuss surface segregation phenomena in $Pt_{75}Ni_{25}$, $Pt_{75}Re_{25}$, and $Pt_{80}Mo_{20}$ nanoparticles in much detail. $Pt_{75}Ni_{25}$ was chosen because nanoparticle catalysts with the exact same composition have been experimentally investigated and found to have enhanced catalytic performance compared to pure Pt [24]. We found from our previous studies [22,23] that $Pt_{75}Re_{25}$ and $Pt_{80}Mo_{20}$ nanoparticles have some distinct surface features, which could be very beneficial for catalysts, in comparison to the Pt-Re and Pt-Mo nanoparticles with other compositions. As discussed in the following sections, these three alloys exhibit different types of surface segregation processes. From phase diagrams [48], it is known that the bulk $Pt_{75}Ni_{25}$, $Pt_{75}Re_{25}$, and $Pt_{80}Mo_{20}$ alloys have fcc crystal structures. Hence, we assumed that their bimetallic nanoparticles also have an fcc crystal structure as well as a cubo-octahedral shape (shown in Fig. 1), which is bounded by {111} and {100} facets. The cubo-octahedron (or incomplete cubo-octahedron when in contact with some supports) is believed to be the equilibrium shape for fcc nanoparticles [49]. Indeed, Pt-Ni [24] and Pt-Ru [50] nanoparticles were found to adopt this shape.

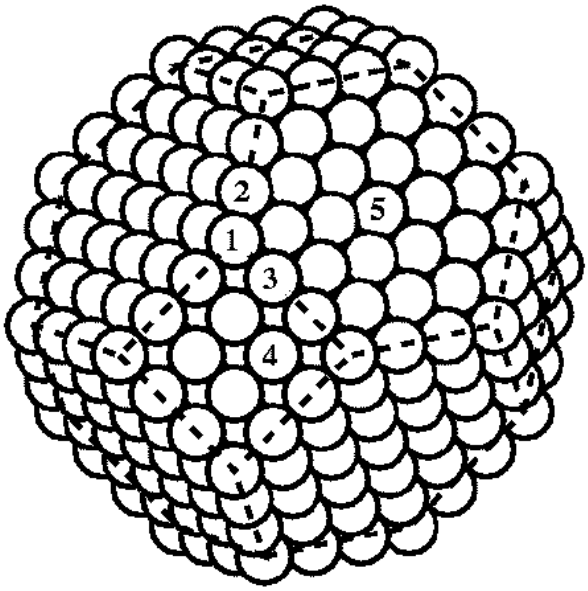

Figure 1. A fcc cubo-octahedral nanoparticle. The numbers label atoms at non-equivalent surface sites in the outermost layer of the particle. They have different numbers of nearest neighbors: atom 1: vertex (six nearest neighbors); atom 2: {111}/{111} edge (seven nearest neighbors); atom 3: {111}/{100} edge (seven nearest neighbors); atom 4: {100} facet (eight nearest neighbors); and atom 5: {111} facet (nine nearest neighbors).

Figure 2 shows that for cubo-octahedral nanoparticles the surface/volume ratio varies nonlinearly with their sizes. The smaller the nanoparticles are, the larger their surface/volume ratios. In typical samples of Pt alloy nanoparticles, the Pt-Ni [24] and Pt-Ru [51] nanoparticles were found to have a size distribution from 2.0 nm to 6.0 nm and the Pt-Mo [52] nanoparticles were found to have an average size of 3.0 nm. Hence, we simulated the surface segregation in Pt-M nanoparticles with four different sizes in a range of particle diameter from about 2.5 to 5.0 nm, which corresponds to a range of surface/volume ratio from about 46 % to 27 %, and a range of total number of atoms from 586 to 4033. We constructed the nanoparticles with "magic numbers" of atoms, for which atomic shells are complete. This minimizes the diffusion of atoms outside the surface, which would unnecessarily consume much computer time (our exchange mechanism achieves the same purpose of long-range hopping).

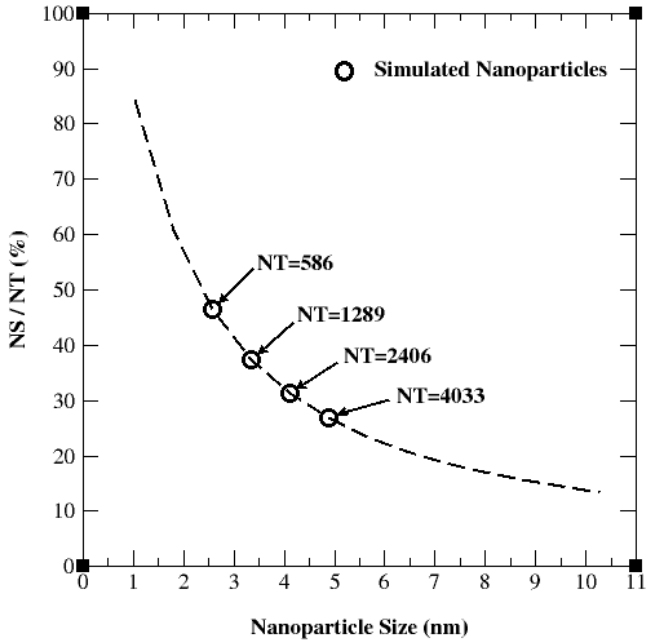

Figure 2. Variation of the number of surface atoms (NS) over the total number of atoms (NT) as a function of the size of perfect fcc cubo-octahedral nanoparticles. We assume for this plot that the nearest separation between two atoms is 2.77 Å, which is the equilibrium nearest separation in pure bulk Pt. The circles represent the nanoparticles for which we performed MC simulations.

Metallic nanoparticles are most often fabricated through the chemical reduction of the metal ions to their elemental states in homogenous solutions [53]. The final configurations of metallic nanoparticles are formed during the reduction process. In this work, we chose a simulation temperature of 600 K, which is close to the experimental reduction temperature of Pt-M nanoparticles and some previous MC simulations of bimetallic nanoparticles [34]. In our MC simulations, the cubo-octahedral Pt-M ($Pt_{75}Ni_{25}$, $Pt_{75}Re_{25}$, and $Pt_{80}Mo_{20}$) nanoparticles were initially constructed with the lattice constants of the bulk alloys with the same composition and with randomly distributed Pt and M atoms. The lattice constants of the disordered fcc Pt-M bulk alloys are determined from a zero average pressure, three-dimensional periodic simulation using MC. For each nanoparticle, we performed MC simulations for multimillion steps. During the MC simulations, both the atomic positions and the distribution of the metal atoms in the

nanoparticles were allowed to change. As a result, both shape relaxation and surface segregation of nanoparticles can occur.

3.2. Equilibrium $Pt_{75}Ni_{25}$ nanoparticles

As shown in Table 1, Pt and Ni have a large difference in atom size in their pure fcc crystal structures. As a result, sufficient atomic relaxation is an important factor for accurately calculating surface segregation in $Pt_{75}Ni_{25}$ nanoparticles. Therefore, we performed MC simulations allowing both atomic displacement and exchange of element types for 4×10^7 MC steps at T=600 K [21]. In Fig. 3, we show exterior and cross-sectional views that expose the outermost surface and centers of equilibrated nanoparticles containing 586 atoms. These views qualitatively reveal a "surface-sandwich structure" for the equilibrium $Pt_{75}Ni_{25}$ nanoparticles. Here, "surface-sandwich structure" implies that the Pt atoms are enriched in the outermost and third atomic layers, while the Ni atoms are enriched in the second atomic layer. This surface-sandwich structure in cubo-octahedral nanoparticles terminated with {111} and {100} facets is in agreement with the experimentally observed oscillatory segregation behavior for the extended (111) and (100) surfaces of Pt-Ni alloys [54].

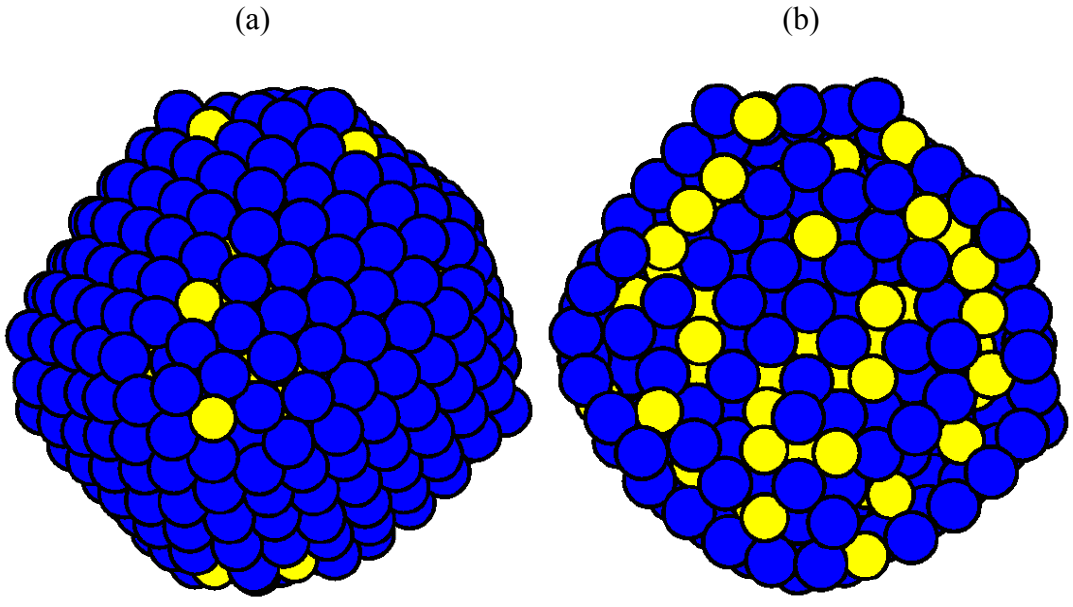

Figure 3. (color) Snapshots of equilibrium $Pt_{75}Ni_{25}$ nanoparticles containing 586 atoms simulated at T=600 K: (a) exterior and (b) [001] cross-sectional views. The blue circles represent the Pt atoms and the bright yellow circles stand for the Ni atoms.

We plot in Fig. 4 our calculated concentrations of Pt atoms in the outermost three atomic layers of the four simulated $Pt_{75}Ni_{25}$ nanoparticles. To eliminate the influence of the initial arbitrary structures, we calculated the concentrations of Pt atoms by averaging values sampled every 10^4 MC steps in the last 2×10^7 MC simulation steps. Our results show that the Pt concentration is nearly 100 at. % in the outermost layer of $Pt_{75}Ni_{25}$ nanoparticles. This theoretical prediction quantitatively agrees with a direct measurement for annealed $Pt_{75}Ni_{25}$ polycrystal surfaces [26] and partially explains the observed enhancement in catalytic performance of $Pt_{75}Ni_{25}$ nanoparticles in comparison to pure Pt nanoparticles [24]. In these equilibrium $Pt_{75}Ni_{25}$ nanoparticles, the Pt concentration in the outermost layer is about 50 at. % higher than in the second atomic layer; and the Pt concentration in the third atomic layer is about 75 at. %. The difference of Pt concentration between these different layers exceeds 20 at. %. The concentration of Pt atoms in the second layer of $Pt_{75}Ni_{25}$ nanoparticles is about 25 at. % lower than the overall concentration of 75 at. % and increases gradually with nanoparticle size. This implies that the extent of Ni enrichment in the second layer of these nanoparticles can be controlled by varying the nanoparticle size.

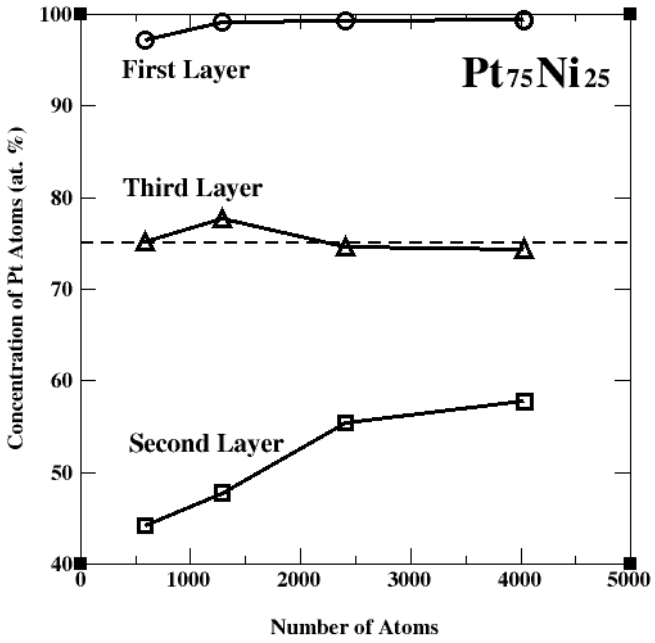

Figure 4. Calculated Pt concentrations in the first (outermost), second, and third layers as a function of the number of atoms in $Pt_{75}Ni_{25}$ nanoparticles, from MC simulations at T=600 K. The dashed line indicates the overall Pt concentration in the nanoparticles.

3.3. Equilibrium $Pt_{75}Re_{25}$ nanoparticles

Inside fcc cubo-octahedral nanoparticles, each atom has twelve nearest neighbors (neglecting relaxations). In contrast, atoms in the outermost (first) layer of the nanoparticles have an incomplete set of nearest neighbors (see Fig. 1). Hence, it is possible to distinguish the core (internal part) and the shell (outermost surface layer) of cubo-octahedral nanoparticles. In equilibrium bimetallic nanoparticles, the core and shell might have different compositions because of surface segregation. Figure 5 shows a strong core-shell structure (Pt is enriched in the shell and correspondingly depleted in the core) of equilibrated $Pt_{75}Re_{25}$ nanoparticles in exterior and cross-sectional views. To obtain the equilibrium structures of $Pt_{75}Re_{25}$ nanoparticles, we performed MC simulations allowing both atomic displacement and exchange of element types for $2x10^7$ MC steps at T=600 K [22].

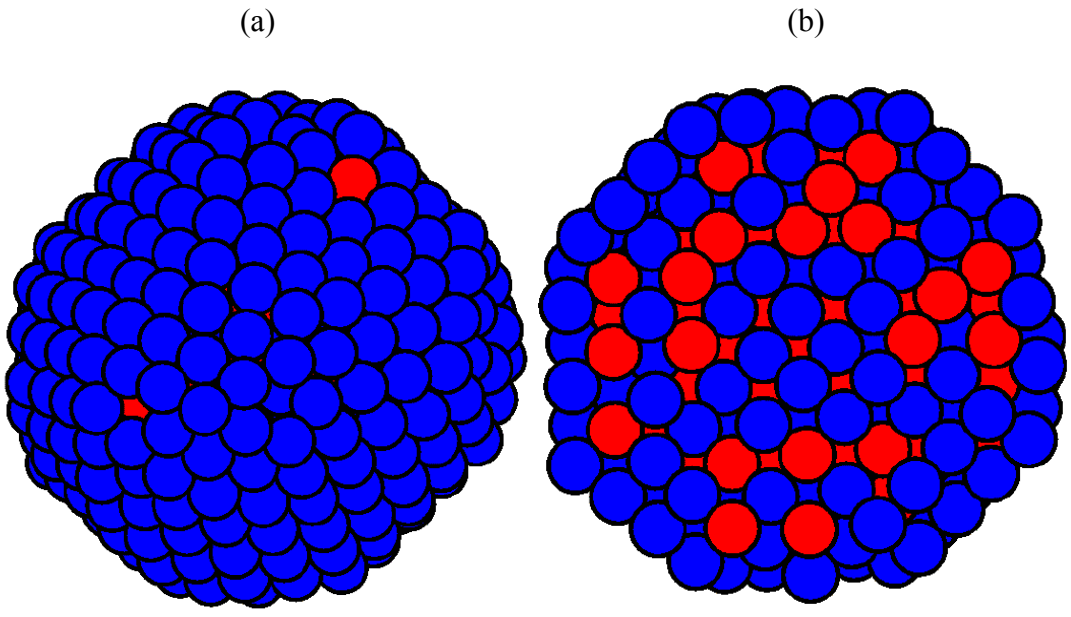

Figure 5. (color) Snapshots of equilibrium $Pt_{75}Re_{25}$ nanoparticles containing 586 atoms simulated at T=600 K: (a) exterior and (b) [001] cross-sectional views. The blue circles represent the Pt atoms and the red circles stand for the Re atoms.

Quantifying the composition difference of the core and shell of these nanoparticles, we calculated the concentrations of Pt atoms in the core and shell by averaging values sampled every 10^4 MC steps in the last $1x10^7$ MC steps. Figure 6 shows the calculated concentrations of Pt atoms in the shell and core. It is found, for equilibrium $Pt_{75}Re_{25}$ nanoparticles, that the shell is composed of almost 100 at. % Pt atoms and hence the core contains fewer Pt atoms. The difference of Pt concentrations in the shell and core can be as high as 42 at. % for $Pt_{75}Re_{25}$ nanoparticles containing 586 atoms. Our finding of equilibrium $Pt_{75}Re_{25}$ nanoparticles with a strong Pt-rich shell and a Re-rich core is consistent with a previous theoretical study that calculated the segregation profiles of irregular shaped Pt-Re particles [55]. It is noticed in Fig. 6 that the Pt concentration in the $Pt_{75}Re_{25}$ nanoparticle cores increases with nanoparticle size. This is because there are more Pt atoms than surface positions in larger nanoparticles, due to a diminishing surface-to-volume ratio. After a pure Pt shell is formed, a growing concentration of Pt atoms is left in the core of larger nanoparticles.

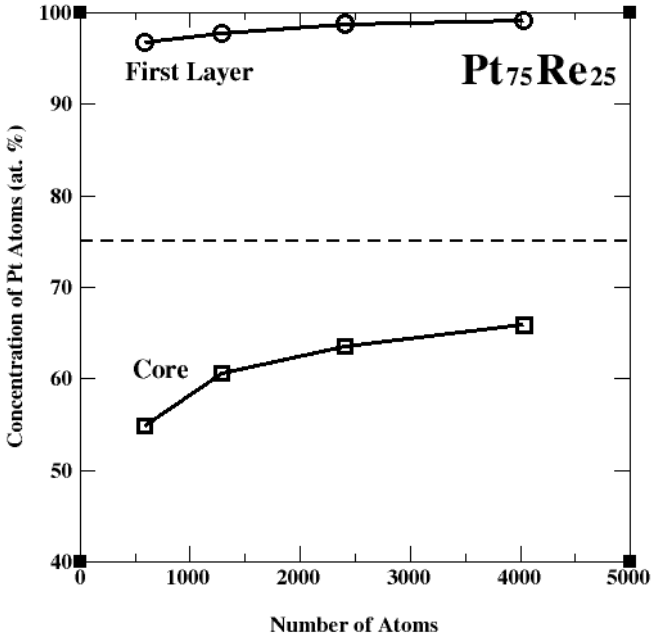

Figure 6. Calculated Pt concentrations in the first (outermost) surface layer and the core region as a function of the number of atoms in $Pt_{75}Re_{25}$ nanoparticles, from MC simulations at T=600 K. The dashed line indicates the overall Pt concentration in the nanoparticles.

3.4. Equilibrium $Pt_{80}Mo_{20}$ nanoparticles

For $Pt_{80}Mo_{20}$ nanoparticles, we performed MC simulations for 1×10^7 steps at T=600K [23]. We show in Fig. 7 final snapshots of equilibrated $Pt_{80}Mo_{20}$ nanoparticles containing 586 atoms from our MC simulations. These plots qualitatively show that Pt atoms are weakly enriched in the surface of these nanoparticles and the Mo atoms preferentially occupy the low-coordination edge and vertex sites in the surface, avoiding Mo-Mo bonds. Thus, the facets are fully occupied by Pt atoms, the Mo atoms only appear at the edges and vertices, and the Pt and Mo atoms arrange themselves in an alternating sequence to achieve a maximal number of Pt-Mo pairs along the edges and vertices.

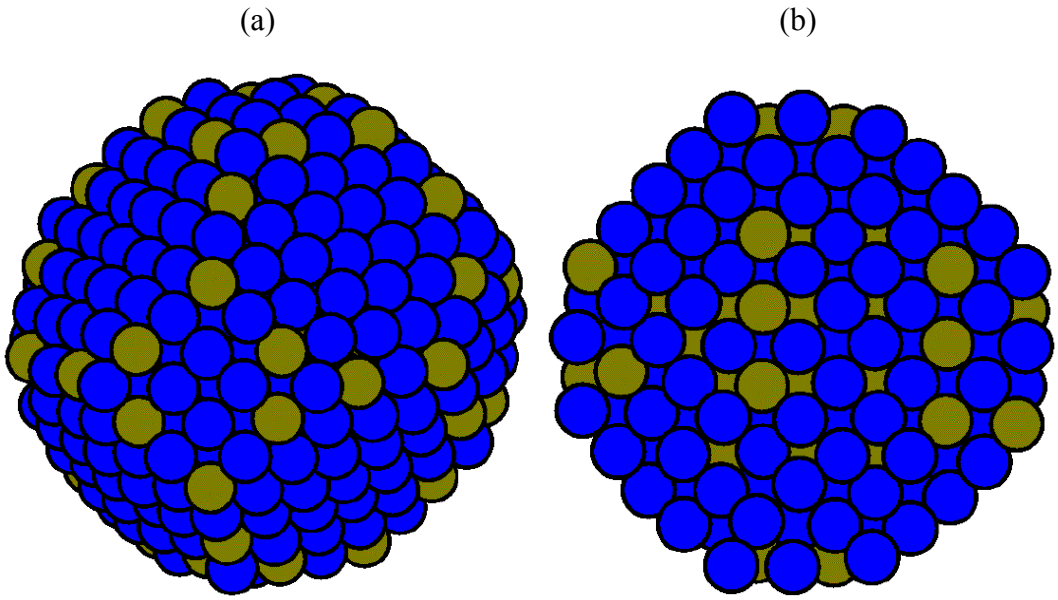

Figure 7. (color) Snapshots of the equilibrium $Pt_{80}Mo_{20}$ nanoparticles containing 586 atoms simulated at T=600 K: (a) exterior and (b) [001] cross-sectional views. In the snapshots, the blue circles represent the Pt atoms and the dark yellow circles stand for the Mo atoms.

To quantitatively characterize the weak surface segregation in the equilibrium $Pt_{80}Mo_{20}$ nanoparticles, we calculated the Pt concentration in their shell and core by averaging the values sampled every 10^3 steps in the last 5×10^6 steps of the MC simulations. In Fig. 8, we plot the calculated Pt concentration in the outermost layer and the inside core. We observe the following two trends from these results. First, the Pt concentrations in the shells are 5 to 11 at. % higher than the Pt concentrations in the cores

of $Pt_{80}Mo_{20}$ nanoparticles. This weak enrichment of Pt atoms in the nanoparticle surfaces is consistent with the experimental finding that the Pt enrichment in the outermost surface layer of $Pt_{70}Mo_{30}$ polycrystals annealed at 970 K is only about 7 at. % [56]. Second, the extent of Pt segregation to the surfaces increases with nanoparticle size. The surface Pt concentration of the $Pt_{80}Mo_{20}$ nanoparticles containing 586 atoms is about 7 at. % lower than for those containing 4033 atoms. This is caused by the inhomogeneous distribution of the Pt atoms in the equilibrium $Pt_{80}Mo_{20}$ nanoparticle surfaces. As shown in Fig. 7, the Pt atoms preferentially segregate to the high-coordination surface sites, namely within the {111} and {100} facets. Since the larger fcc cubo-octahedral nanoparticles have a higher ratio of {111} and {100} facet sites vs. edge and vertex sites [49], the preferential segregation of Pt atoms to the facet sites causes a higher Pt concentration in the surface of large nanoparticles than small ones.

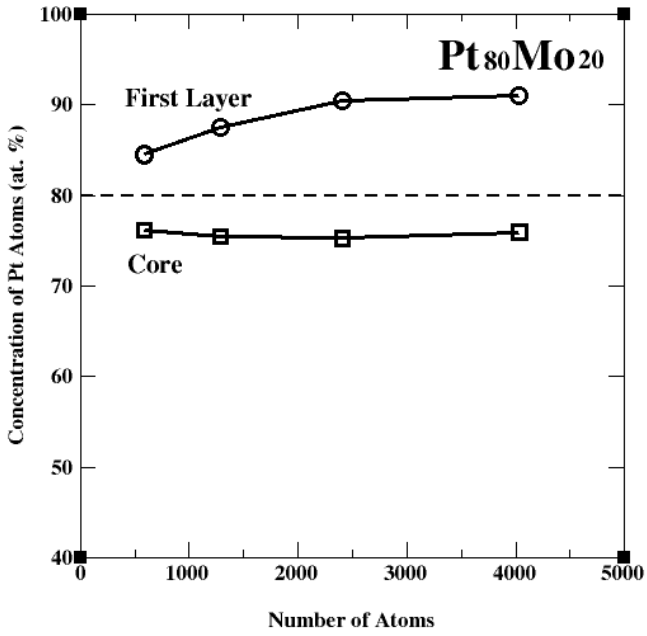

Figure 8. Calculated Pt concentrations in the first (outermost) surface layer and the core region as a function of the number of atoms in $Pt_{80}Mo_{20}$ nanoparticles, from MC simulations at T=600 K. The dashed line indicates the overall Pt concentration in the nanoparticles.

4. Discussion

4.1. Facet reconstruction processes in equilibrium Pt-M nanoparticles

In comparison to bulk-terminated fcc cubo-octahedrons (shown in Fig. 1), the equilibrium $Pt_{75}Ni_{25}$ (Fig. 3(a)), $Pt_{75}Re_{25}$ (Fig. 5(a)), and $Pt_{80}Mo_{20}$ (Fig. 7(a)) nanoparticles appear to be much rounder. This is because, to lower the energy, the atoms at the low-coordination sites (edges and vertices) relax inward more than those at the facet sites. Such relaxations are familiar at "rough" extended surfaces [57], in particular for fcc(110), fcc(211) and fcc(210), which contain atoms with the same local geometry as the nanoparticle edge and vertex atoms of types 2, 3, and 1 (as shown in Fig. 1), respectively.

Furthermore, we observed in our MC simulations a reconstruction process in {100} facets of the relaxed $Pt_{75}Ni_{25}$ and $Pt_{75}Re_{25}$ cubo-octahedral nanoparticles. Compared to the original square lattice of the (100) facet in the cubo-octahedron shown in Fig. 1, the 4×4 atoms in the (100) facet of $Pt_{75}Ni_{25}$ (Fig. 3(a)) and $Pt_{75}Re_{25}$ (Fig. 5(a)) nanoparticles tend to arrange themselves into a denser hexagonal configuration together with some atoms coming from inside the nanoparticles. The reconstruction of the {100} facets from a square to hexagonal lattice in the Pt enriched shell of nanoparticles is reasonable: indeed, the (100) surface of pure elemental Pt undergoes a similar reconstruction to a hexagonal outermost layer [57-59]. Also, it has been observed for Pt-Ni alloys that the top layer of the (100) surface can reconfigure itself to such a hexagonal arrangement of atoms [60,61]. Interesting is our prediction that such a reconstruction may take place on facets as small as 4x4 atoms, despite the perturbing effects of the surrounding edges and vertices.

However, we did not observe this reconstruction process in our MC simulations for the {100} facets in equilibrium $Pt_{80}Mo_{20}$ nanoparticles. Figure 7(a) shows an unreconstructed {100} facet that keeps its square lattice after 10^7 MC simulation steps in the $Pt_{80}Mo_{20}$ nanoparticle. We notice that there are some Mo atoms in the edges surrounding the unreconstructed {100} facet in Fig. 7(a). In contrast, there are nearly no Ni or Re atoms in the {100} facets of the equilibrium $Pt_{75}Ni_{25}$ and $Pt_{75}Re_{25}$ cubo-octahedral nanoparticles due to the strong segregation of Pt atoms to the surfaces. It thus appears that Mo atoms in {100} facets prevent the reconstruction from happening, while pure-Pt facets do reconstruct.

4.2. Different surface segregation phenomena in equilibrium Pt-M nanoparticles

Figures 4, 6, and 8 show clearly that surface segregation phenomena are distinctly different in cubo-octahedral nanoparticles for three different Pt-M alloys: the surface-sandwich structure for $Pt_{75}Ni_{25}$, the strong core-shell structure for $Pt_{75}Re_{25}$, and the weak core-shell structure for $Pt_{80}Mo_{20}$. The three types of surface segregation in Pt-M nanoparticles can be explained qualitatively using the heats of solution of alloys, atom sizes of pure elements, and relative surface energies of pure elements.

(1) From Table 1 for pure Pt and pure Ni, we see that the surface energies are very close but the atom sizes (proportional to the lattice constant of fcc crystals) are quite different. Pt atoms are about 11 % larger than Ni atoms. Thus, segregating Pt atoms to the close-packed surfaces, such as (111) and (100), of Pt-Ni alloys lowers the strain energy without changing the surface energy. In addition, the heat of solution of $Pt_{75}Ni_{25}$ alloys is negative so that a $Pt_{75}Ni_{25}$ solid solution is formed. Our MEAM potentials lead to a cohesive energy for ordered Pt_3Ni ($L1_2$) of –0.080 eV, which is close to our first-principles calculation result of –0.079 eV [21]. The strong bonding tendency between Pt and Ni atoms leads to an oscillatory surface segregation pattern in $Pt_{75}Ni_{25}$ nanoparticles: after Pt segregates to the outermost surface layer, Ni will segregate to its sublayer to form Pt-Ni bonds and decrease the total energy. However, the Pt-Ni bonds are not strong enough to induce ordering in the core of nanoparticles at T=600K.

(2) The equilibrium crystal structure of Re is hcp. Our MEAM potential for Re predicts that hcp Re is more stable by 0.084 eV/atom than fcc Re, whose equilibrium lattice constant is 3.89 Å [22]. We also calculated the surface energies for the relaxed extended surfaces of fcc Re using the MEAM potential. Our results are: 3786 mJ/m^2 for (111), 4174 mJ/m^2 for (100), and 3678 mJ/m^2 for (110) [22]. Comparing these results for fcc Re to the data for fcc Pt in Table 1, we found that fcc Pt and fcc Re atoms have similar atomic sizes but dramatically different surface energies. The surface energies of fcc Re are about two times larger than those of fcc Pt. Therefore, segregating Pt atoms to the surfaces will lead to a lower energy configuration of fcc $Pt_{75}Re_{25}$ nanoparticles. The large difference (about 2000 mJ/m^2) for surface energies between fcc Pt and fcc Re

accounts for the observed strong segregation of Pt atoms to the $Pt_{75}Re_{25}$ nanoparticle surfaces.

(3) The equilibrium crystal structure of Mo is bcc. It is found from both the MEAM potentials and first-principles calculations that fcc Mo is unstable and will transform to lower energy structures under the volume-conserving tetragonal deformation [23]. The lowest-energy metastable fcc Mo from our MEAM potential has a cohesive energy of 0.32 eV higher than that of bcc Mo, and a lattice constant of 4.01 Å (slightly larger than 3.92 Å for equilibrium fcc Pt) [23]. Moreover, we evaluated the surface energies of the *unrelaxed* extended surfaces of fcc Mo. Our results are: 2535 mJ/m^2 for (111), 2790 mJ/m^2 for (100), and 2822 mJ/m^2 for (110). Further, our MEAM potential predicts that the cohesive energy of ordered Pt_3Mo ($L1_2$) is –0.093 eV, similar to our first-principles calculation [23]. Consequently, for $Pt_{80}Mo_{20}$ nanoparticles, a negative heat of alloy formation favors the solution element (Pt) segregating to the surfaces; similarly, lower surface energies for Pt also favor a segregation of Pt atoms to the surface, while strain energy considerations favor the larger Mo atoms segregating to the surfaces. A combination of these three factors leads to Pt atoms segregating to the surface of $Pt_{80}Mo_{20}$ nanoparticles. Since the differences in atom size and surface energies for fcc Pt and fcc Mo are rather small, Pt atoms just slightly segregate to the nanoparticle surfaces as plotted in Fig. 8: a weak core-shell structure is formed.

4.3. Surface segregation in equilibrium Pt-M nanoparticles with other compositions

In our previous work [21-23], we have also investigated surface segregation in equilibrium Pt-M nanoparticles with other compositions. We next discuss some interesting features of surface segregation phenomena found in those nanoparticles.

Unlike in extended bulk surfaces, surface segregation in nanoparticles is often limited by the availability of the segregating atoms because the nanoparticles contain a finite number (several thousands) of atoms. This phenomenon is most prominent in Re rich Pt-Re alloy nanoparticles. In Ref. [22], we simulated the surface segregation process in $Pt_{25}Re_{75}$ nanoparticles assuming a truncated hexagonal bipyramidal shape and an hcp crystal structure. Pt atoms segregate strongly to the surface of Pt-Re nanoparticles. Since there are more surface sites than surface-segregating Pt atoms in the small $Pt_{25}Re_{75}$

nanoparticles, nearly all Pt atoms in the nanoparticles will segregate to the surface. As a result, Pt concentrations on the surface of the small Pt-Re nanoparticles with a low Pt concentration are strongly dependent of the overall Pt concentration in the nanoparticles [22].

The interplay of surface segregation and crystal ordering in alloys could lead to a significant deviation in surface segregation behavior from the predictions for randomly disordered alloys. The resulting new phenomena include segregation suppression (or increase), oscillatory segregation profiles, surface-induced order, and surface-induced disorder [3]. Pt-Ni alloys have a strong ordering tendency, hence we found an oscillatory segregation profile in Pt-Ni nanoparticles [21]. The interdependence of segregation and ordering in alloy nanoparticles can manifest itself in a new way: surface segregation behavior depends on nanoparticle size. In Ref. [21], we described MC simulations for cubo-octahedral $Pt_{50}Ni_{50}$ nanoparticles at T=600 K. We noticed that the two smaller nanoparticles (containing 586 and 1289 atoms) assume the surface sandwich structure, while the two larger nanoparticles (containing 2406 and 4033 atoms) adopt the core-shell structure: Pt is enriched only in the outermost shell and Pt concentrations are similar elsewhere in the core. For bulk $Pt_{50}Ni_{50}$ alloys, the disordered fcc structure will change to the ordered $L1_0$ structure below 900K [62]. It is known that the order-disorder transition temperature of nanoparticles is a function of their size and shape [63,64]. The transition temperature would be higher for larger nanoparticles, therefore, the simulation temperature of 600 K might be below the order-disorder transition temperatures of larger $Pt_{50}Ni_{50}$ nanoparticles while above the order-disorder transition temperatures of smaller $Pt_{50}Ni_{50}$ nanoparticles. We indeed observed ordered PtNi clusters in the core of the two simulated larger nanoparticles. We anticipate that a similar size-dependent surface segregation behavior will occur for $Pt_{75}Ni_{25}$ nanoparticles with a much larger number of atoms, since bulk $Pt_{75}Ni_{25}$ alloys has a lower order-disorder transition temperature (800 K) than $Pt_{50}Ni_{50}$ alloys.

The facet, edge, and vertex atoms in nanoparticle surfaces have different local environments, shown as the various surface atom sites in Fig. 1. Atoms will have segregation energies at different surface sites. Therefore, if the segregating atoms do not achieve a concentration of 100 at. % in the outermost surface of nanoparticles, they

would have different concentrations at various surface sites due to preferential segregation. For example, Pt atoms preferentially segregate to the surface sites with a lower coordination number, i.e., Pt atoms would segregate most to vertices, less to edges, and least to facets of hcp $Pt_{25}Re_{75}$ nanoparticles; the discrepancy in Pt concentrations at various surface sites can be as large as 60 at. % [22]. In contrast, we found from our simulations that Pt atoms preferentially segregate to the surface sites with a higher coordination number, i.e., Pt atoms would segregate most to facets of fcc Pt-Mo nanoparticles [23]. It is difficult for phenomenological theories to predict the preferential segregation in Pt-M nanoparticles by only considering thermodynamic properties of bulk alloys.

5. Conclusions

We have developed and applied a quantitative approach to investigating the segregation of Pt atoms to the surfaces of equilibrium fcc cubo-octahedral $Pt_{75}Ni_{25}$, $Pt_{75}Re_{25}$, and $Pt_{80}Mo_{20}$ nanoparticles at 600 K. Our approach is comprised of the Modified Embedded Atom Method for energy evaluation and the Monte Carlo method as the model of statistical mechanics.

We found from our simulations that:

(1) Due to the surface segregation resulting from a large atomic size difference and a strong ordering tendency of Pt and Ni, $Pt_{75}Ni_{25}$ nanoparticles form a surface-sandwich structure in which the Pt atoms are strongly enriched in the outermost and third layers while the Ni atoms are enriched in the second layer. Particularly in Pt-rich nanoparticles, a nearly pure Pt outermost surface layer can be achieved;

(2) Due to the strong surface segregation that is caused by the significant surface energy difference between Pt and Re, the equilibrium $Pt_{75}Re_{25}$ nanoparticles adopt a core-shell structure: a nearly pure Pt shell surrounding a more homogeneous Pt-Re core;

(3) In $Pt_{80}Mo_{20}$ nanoparticles, the Pt atoms are seen to weakly segregate to the surface. Hence, a mixture of Pt and Mo atoms is found on the nanoparticle surfaces. However, the Pt and Mo atoms are not distributed uniformly in this outermost atomic layer: instead, the Pt atoms segregate preferentially to the facet sites, less to edge sites,

and least to vertex sites, while Mo atoms favor the edge and vertex sites, alternating with Pt whenever possible.

Our simulations of surface segregation in nanoparticles quantitatively agree with previous experimental and theoretical results for extended surfaces of Pt-Ni, Pt-Re, and Pt-Mo alloys. Therefore, we believe that our quantitative approach is reliable and should have wide applicability in predicting surface segregation in multicomponent alloy nanoparticles, which is particularly helpful in designing catalysts in the nanoscale. We can take advantage of such an approach to design alloy nanoparticle catalysts in which due to surface segregation precious component metals are enriched in the outermost surfaces; the atoms in the sublayers electronically enhance the catalytic performance; and various atoms arrange themselves to some particular patterns to increase the selectivity of catalysts.

Acknowledgment. This work was supported by the Office of Science, Materials Sciences Division, of the U.S. Department of Energy under Contract Nos. DE-AC03-76SF00098 at LBNL and W-7405-ENG-36 at LANL. The computations were carried out at the National Energy Research Scientific Computing Center (NERSC), which is operated by LBNL for the U.S. Department of Energy.

References

[1] P.A. Dowben and A. Miller (Eds.), Surface Segregation Phenomena, CRC Press, Boca Raton, Florida, 1990.

[2] J.A. Rodriguez, Surf. Sci. Rep. 24 (1996) 223.

[3] M. Polak, L. Rubinovich, Surf. Sci. Rep. 38 (2000) 127.

[4] D. Mclean, Grain Boundaries in Metals, Oxford University Press, Oxford, 1957.

[5] F.L. Williams, D. Nason, Surf. Sci. 45 (1974) 377.

[6] A.R. Miedema, Z. Metallk, 69 (1978) 455.

[7] M.J. Kelly, V. Ponec, Prog. Surf. Sci. 11 (1981) 139.

[8] S. Mukherjee, J.L. Morán-López, Surf. Sci. 188 (1987) L742.

[9] S.M. Foiles, in: P.A. Dowben and A. Miller (Eds.), Surface Segregation Phenomena, CRC Press, Boca Raton, Florida, 1990, pp. 79-106.

[10] A.V. Ruban, H.L. Skriver, J.K. Nørskov, Phys. Rev. B 59 (1999) 15990.

[11] M.I. Baskes, Phys. Rev. B 62 (1992) 2727.

[12] M.I. Baskes and R.A. Johnson, Modell. Simul. Mater. Sci. Eng. 2 (1994) 147.

[13] N. Metropolis, A.W. Rosenbluth, M.N. Rosenbluth, A.H. Teller, and E. Teller, J. Chem. Phys. 21 (1953) 1087.

[14] S. Link, M.A. El-Sayed, J. Phys. Chem. B 103 (1999) 8410.

[15] P.V. Kamat, J. Phys. Chem. B 106 (2002) 7729.

[16] L.C. Varanda, M.P. Morales, G.F. Goya, M. Imaizumi, C.J. Serna, M. Jafelicci Jr., Mater. Sci. Eng. B 112 (2004) 188.

[17] G.A. Somorjai and Y.G. Borodko, Catal. Lett. 1 (2001) 76.

[18] W. Fritzsche, T.A. Taton, Nanotechnology 14 (2003) R63.

[19] N.M. Marković, P.N. Ross, Surf. Sci. Rep. 45 (2002) 117.

[20] J.K. Nørskov, J. Rossmeisl, A. Logadottir, L. Lindqvist, J.R. Kitchin, T. Bligaard, H. Jónsson, J. Phys. Chem B 108 (2005) 17886.

[21] G. Wang, M.A. Van Hove, P.N. Ross, M.I. Baskes J. Chem. Phys. 122 (2005) 024706.

[22] G. Wang, M.A. Van Hove, P.N. Ross, M.I. Baskes J. Chem. Phys. 121 (2004) 5410.

[23] G. Wang, M.A. Van Hove, P.N. Ross, M.I. Baskes J. Phys. Chem. B 109 (2005) 11683.

[24] U.A. Paulus, A. Wokaun, G.G. Scherer, T.J. Schmidt, V. Stamenković, V. Radmilovic, N.M. Marković, P.N. Ross, J. Phys. Chem. B 106 (2002) 4181.
[25] B.N. Grgur, N.M. Markovic, P.N. Ross, Electrochimica Acta. 43 (1998) 3631.
[26] V. Stamenković, T.J. Schmidt, P.N. Ross, N.M. Marković, J. Phys. Chem. B 106 (2002) 11970.
[27] J.R. Kitchin, J.K. Nørskov, M.A. Barteau, J.G. Chen, J. Chem. Phys. 120 (2004) 10240.
[28] B.N. Grgur, N.M. Markovic, P.N. Ross, J. Electrochem. Soc. 146 (1999) 1613.
[29] T.E. Shubina, M.T.M. Koper, Electrochim. Acta 47 (2002) 3621.
[30] N. Toshima, T. Yonezawa, New J. Chem. 22 (1998) 1179.
[31] E.A. Stern, S.M. Heald, in: E.E. Koch (Ed.), Handbook of Synchrotron Radiation, North-Holland, Amsterdam, 1983, Chapter 10.
[32] U. Kolb, S.A. Quaiser, M. Winter, M.T. Reetz, Chem. Mater. 8 (1996) 1889.
[33] M.S. Nashner, A.I. Frenkel, D. Somerville, C.W. Hills, J.R. Shapley, R.G. Nuzzo, J. Am. Chem. Soc. 120 (1998) 8093.
[34] J.K. Strohl, T.S. King, J. Catal. 116 (1989) 540.
[35] O.L.J. Gijzeman, Appl. Surf. Sci. 64 (1993) 9.
[36] J.L. Rousset, B.C. Khanra, A.M. Cadrot, F.J. Cadete Santos Aires, A.J. Renouprez, M. Pellarin, Surf. Sci. 352-354 (1996) 583.
[37] L. Yang, Phil. Mag. A 80 (2000) 1879.
[38] D.S. Mainardi, P.B. Balbuena, Langmuir 17 (2001) 2047.
[39] A.M Molenbroek, J.K. Nørskov, B.S. Clausen, J. Phys. Chem. B 105 (2001) 5450.
[40] M.S. Daw, M.I. Baskes, Phys. Rev. Lett. 50 (1983) 1285.
[41] M.S. Daw, M.I. Baskes, Phys. Rev. B 29 (1984) 6443.
[42] B.J. Lee, M.I. Baskes, Phys. Rev. B 62 (2000) 8564.
[43] B.J. Lee, M.I. Baskes, H. Kim, Y.K. Cho, Phys. Rev. B 64 (2001) 184102.
[44] L. Vitos, A.V. Ruban, H.L. Skriver, J. Kollár, Surf. Sci. 411 (1998) 186.
[45] W.R. Tyson, W.A. Miller, Surf. Sci. 62 (1977) 267.
[46] F.R. de Boer, R. Room, W.C. Mattens, A.R. Miedema, A.K. Niessen, Cohesion in Metals, North-Holland, Amsterdam, 1988.

[47] M.I. Baskes, J.E. Angelo, C.L. Bisson, Modell. Simul. Mater. Sci. Eng. 2 (1994) 505.

[48] T.B. Massalski (Eds), Binary Alloy Phase Diagrams, ASM International, Materials Park, OH, 1990.

[49] R. Van Hardeveld, F. Hartog, Surf. Sci. 15 (1969) 189.

[50] A.I. Frenkel, C.W. Hills, R.G. Nuzzo, J. Phys. Chem. B 105 (2001) 12689.

[51] C.W. Hills, N.H. Mack, R.G. Nuzzo, J. Phys. Chem B 107 (2003) 2626.

[52] S. Mukerjee, R.C. Urian, S.J. Lee, E.A. Ticianelli, J. McBreen, J. Electrochem. Soc. 151 (2004) A1094.

[53] D.V. Goia, J. Mater. Chem. 14 (2004) 451.

[54] Y. Gauthier and R. Baudoing, in: P.A. Dowben and A. Miller (Eds.), Surface Segregation Phenomena, CRC Press, Boca Raton, Florida, 1990, pp. 169-206.

[55] S. Helfensteyn, C. Creemers, Surf. Sci. 507-510 (2002) 783.

[56] B.N. Grgur, N.M. Marković, P.N. Ross, J. Phys. Chem. B 102 (1998) 2494.

[57] P.R. Watson, M.A. Van Hove, K. Hermann, NIST Surface Structure Database V 5.0, NIST Standard Reference Data Program, Gaithersburg, MD, 2004.

[58] M.A. Van Hove, R.J. Koestner, P.C. Stair, J.P. Bibérian, L.L. Kesmodel, I. Bartoš, G.A. Somorjai, Surf. Sci. 103 (1981) 189.

[59] M.A. Van Hove, R.J. Koestner, P.C. Stair, J.P. Bibérian, L.L. Kesmodel, I. Bartoš, G.A. Somorjai, Surf. Sci. 103 (1981) 218.

[60] Y. Gauthier, R. Baudoing-Savois, J. Rundgren, M. Hammar, M. Gothelid, Surf. Sci. 327 (1995) 100.

[61] W. Hebenstreit, G. Ritz, M. Schmid, A. Biedermann, P. Varga, Surf. Sci. 388 (1997) 150.

[62] C.E. Dahmani, M.C. Cadeville, J.M. Sanchez, and J.L Morán-Lópes, Phys. Rev. Lett. 55 (1985) 1208.

[63] T. Tadaki, A. Koreeda, Y. Nakata, and T. Kinoshita, Surf. Rev. Lett. 3 (1996) 65.

[64] T. Tadaki, T. Kinoshita, Y. Nakata, T. Ohkubo, and Y. Hirotsu, Z. Phys. D 40 (1997) 493.

Table 1. Energies of the relaxed extended low-index surfaces for pure Pt, Ni, Re, and Mo calculated using our MEAM potentials, compared to first-principles results ([a] Ref. [44]) and experiments ([b] Ref. [45] and [c] Ref. [46]). The surface energies are in units of mJ/m^2. The equilibrium lattice types and parameters predicted using the MEAM potentials for pure Pt, Ni, Re, and Mo are given in the second column. The hcp structure has two $(10\bar{1}0)$ surface terminations distinguished by the first interlayer distance d. In the table, $(10\bar{1}0)_A$ refers to the surface with $d=(\frac{\sqrt{3}}{6})a$ while $(10\bar{1}0)_B$ denotes the surface with $d=2(\frac{\sqrt{3}}{6})a$.

Element	Lattice	Surface	MEAM	First-principles [a]	Experiment
Pt	fcc	(111)	1651	2299	2489 [b], 2475 [c]
	a=3.920Å	(100)	2155	2734	
		(110)	1963	2819	
Ni	fcc	(111)	2039	2011	2380 [b], 2450 [c]
	a=3.520Å	(100)	2438	2426	
		(110)	2362	2368	
Re	hcp	(0001)	3955	4214	3626 [b], 3600 [c]
	a=2.764Å	$(10\bar{1}0)_A$	3809	4628	
	c/a=1.608	$(10\bar{1}0)_B$	4343	5985	
Mo	bcc	(110)	1963	2819	2907 [b], 3000 [c]
	a=3.150Å	(111)	3116	3740	
		(100)	3144	3837	

Figures in black and white

Figure 3:

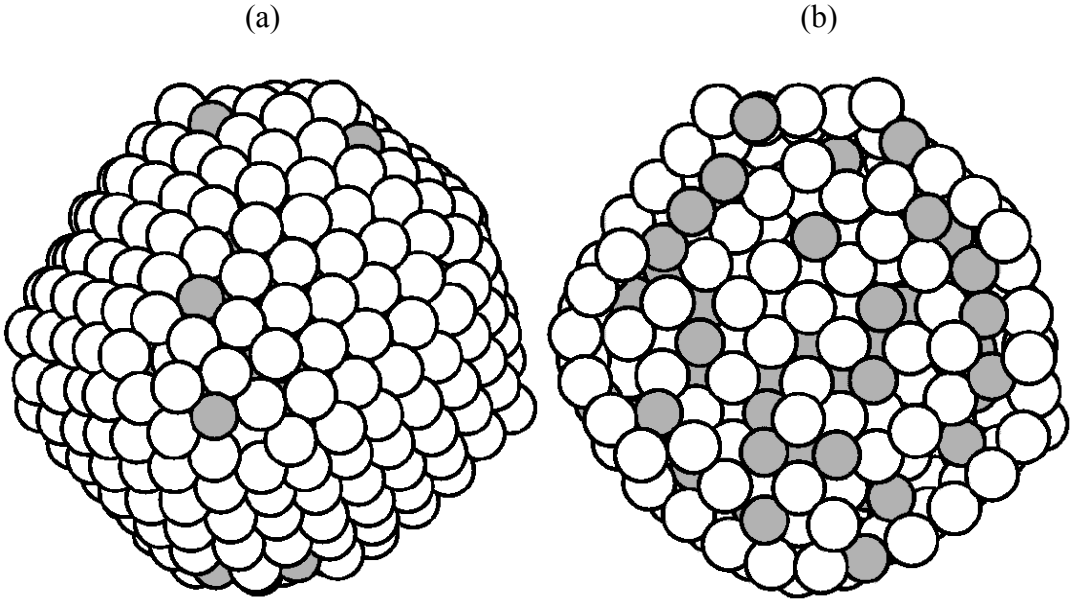

Figure 3. Snapshots of equilibrium $Pt_{75}Ni_{25}$ nanoparticles containing 586 atoms simulated at T=600 K: (a) exterior and (b) [001] cross-sectional views. The open circles represent the Pt atoms and the light gray circles stand for the Ni atoms.

Figure 5:

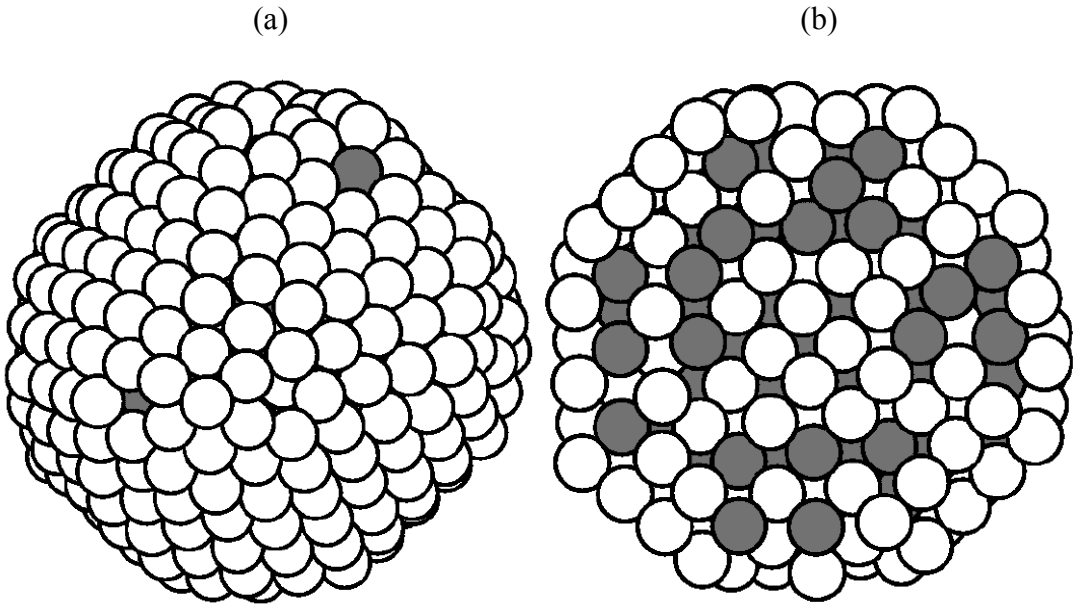

Figure 5. Snapshots of equilibrium $Pt_{75}Re_{25}$ nanoparticles containing 586 atoms simulated at T=600 K: (a) exterior and (b) [001] cross-sectional views. The open circles represent the Pt atoms and the dark gray circles stand for the Re atoms.

Figure 7:

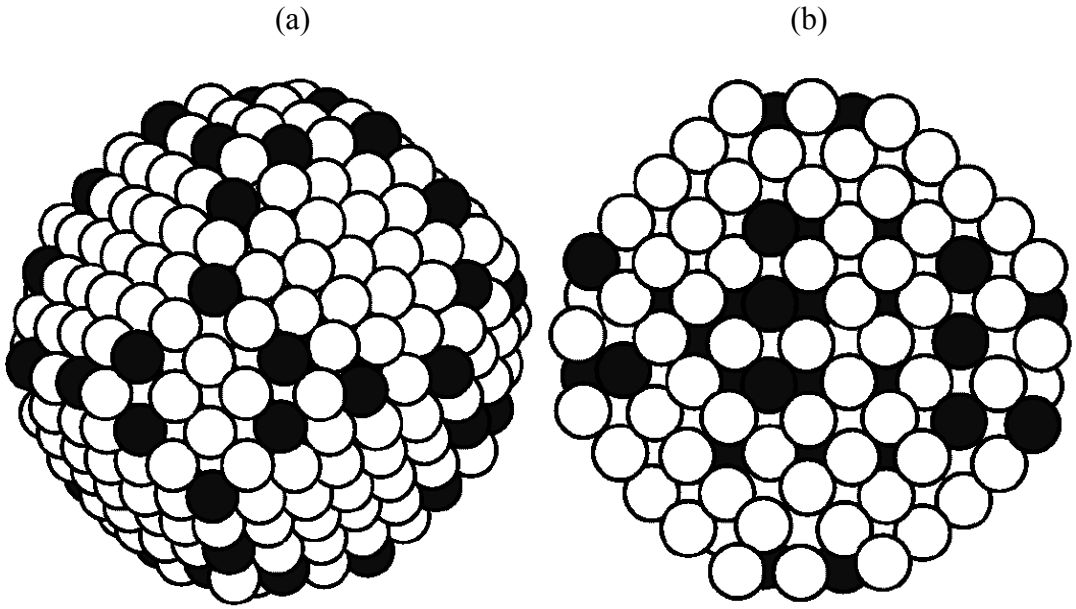

Figure 7. Snapshots of the equilibrium $Pt_{80}Mo_{20}$ nanoparticles containing 586 atoms simulated at T=600 K: (a) exterior and (b) [001] cross-sectional views. In the snapshots, the open circles represent the Pt atoms and the black circles stand for the Mo atoms.